

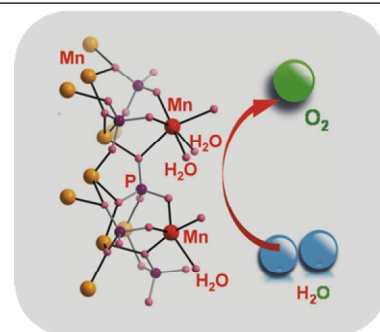
The Mechanism of Water Oxidation from Mn-Based Heterogeneous Electrocatalysts

Shujiao Yang¹, Lingshuang Qin¹, Wei Zhang^{1*} and Rui Cao^{1*}

¹Key Laboratory of Applied Surface and Colloid Chemistry, Ministry of Education, School of Chemistry and Chemical Engineering, Shaanxi Normal University, Xi'an 710119, China

ABSTRACT Searching for a renewable energy system is always the goal to fulfill sustainable development for the future. Water oxidation is considered as a crucial reaction to attain sustainable energy systems. Inspired by the biological Mn_4CaO_5 cluster, considerable effort has been devoted to developing highly efficient Mn-based heterogeneous catalysts and exploring intrinsic mechanism for water oxidation. This review begins with describing the structural characteristics of the Mn_4CaO_5 cluster and the proposed catalytic cycle. Then, the structural characteristics of synthetic Mn-based heterogeneous catalyst are summarized, with emphasis on the understanding of reaction mechanisms and the rate-determining steps. Finally, the strategy of understanding the catalytic mechanism of Mn-based water oxidation is prospected.

Keywords: water oxidation, Mn-based electrocatalysts, oxygen evolution reaction, structure, mechanism



1 INTRODUCTION

With a rising global population, increasing energy demands and impending climate change, major concerns have been raised over the security of our energy future and have motivated a variety of researchers to develop alternative energy.^[1–3] Numerous innovative ideas have been proposed for achieving more efficient energy conversion or storage systems such as water electrolysis, fuel cells and metal-air batteries.^[4–6] They are two-electrode systems in which hydrogen evolution (HER) or oxygen reduction (ORR) occurs at the cathode and oxygen evolution (OER) or oxidation of certain chemical fuels at the anode. Due to sluggish kinetics and complex reaction pathways of water oxidation, including water oxidation activation, O–O bond formation, intermediate peroxide activation and O_2 liberation,^[7,8] it has been considered as a major bottleneck in the development of electrochemical energy conversion and storage system. Therefore, in the past few decades, tremendous efforts have been devoted to understanding the mechanism of this challenging reaction and improving the catalytic activity.^[9] Inspired by the biological photosystem II (PS II), Mn-based materials have been extensively studied as promising candidate catalysts for efficient water oxidation.^[10,11]

In this review, the central structure and catalytic cycle process of water oxidation in nature will first be introduced. Secondly, the structural characteristics of synthetic Mn-based heterogeneous catalyst are summarized, with emphasis on the understanding of reaction mechanisms and rate-determining steps. Finally, the strategy of understanding the catalytic mechanism of Mn-based water oxidation was prospected.

2 THE OXYGEN-EVOLVING CENTER IN PHOTOSYSTEM II (PSII)

In nature, water oxidation is completed by the oxygen-evolving

center (OEC) in PS II.^[12–15] The OEC consists of an inorganic manganese-calcium-oxo cluster (Mn_4CaO_5), which is stabilized by a large number of the surrounding amino acid residues and water molecules (Figure 1a).^[16] The Mn_4CaO_5 central structure and surrounding environment cooperatively perform the water oxidation reaction. Compared with current artificial catalysts, the OEC exhibits more efficient and selective water oxidation catalytic activity, achieving a turnover frequency of 100 s^{-1} for water oxidation with only 150–300 mV of overpotential.^[10] The possible reasons for its high catalytic activity are as follows. First, the Mn_4CaO_5 complex consists of a highly distorted Mn_3Ca -oxo cubane-like motif and one dangling Mn atom (Figure 1b).^[17] When the redox state changes between Mn(III) and Mn(V), this highly distorted structure might promote its atomic rearrangement in the water oxidation reaction. Second, researchers have found that the Ca(II) ion is essential for the high activity of OEC and may have a direct effect on the oxidation process of water.^[18] Third, the hydrogen bond network formed by the surrounding amino acid residues provides well-defined channels for the transfer of substrate water molecules and products such as H^+ and O_2 (Figure 1c).^[17]

In water oxidation reaction, the OEC catalyzes water splitting into electrons, protons and dioxygen through a five-state cycle (Kok cycle, S_n , $n = 0–4$, where n is the number of accumulated oxidizing equivalents) (Figure 1d).^[19,20] During the entire Kok cycle, each Mn atom in the tetrameric cluster is continuously oxidized from Mn(III) to Mn(IV) with simultaneous deprotonation of water. And O–O bond is generated in the $\text{S}_3–\text{S}_4$ step and then O_2 is released in the $\text{S}_4–\text{S}_0$ step. In recent years, the structural changes of Mn_4CaO_5 in each step of the Kok cycle have been determined by femtosecond X-ray free electron laser technology.^[21,22] In addition, the atomic arrangement and oxidation state of S_n state were also revealed in the experiment. Only S_4 state

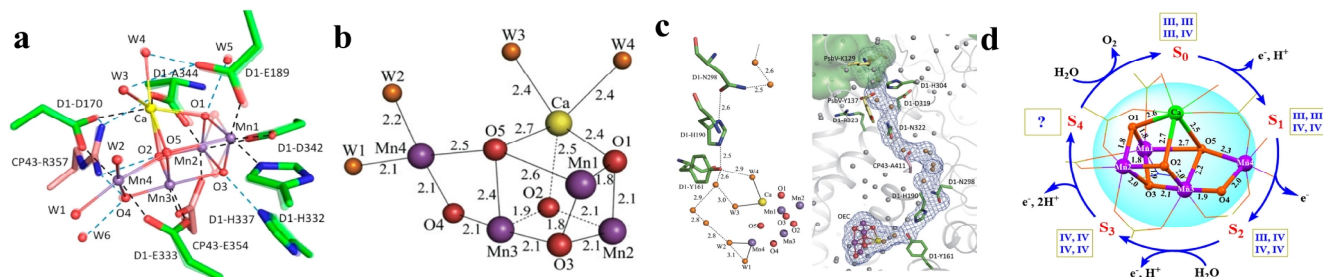


Figure 1. Structure of the Mn_4CaO_5 cluster. (a) Crystal structure of the Mn_4CaO_5 cluster and its ligand environment. Reprinted with permission from ref. 16. Copyright 2017 American Chemical Society. (b) Bond length differences (in Å) between metal atoms and oxo bridges or water molecules. (c) Hydrogen bond network from the Mn_4CaO_5 cluster. Water molecules participating in the hydrogen bond network are depicted in orange, whereas those not participating are in grey. Reprinted with permission from ref. 19. Copyright 2011 Nature Publishing Group. (d) Kok cycle: the five intermediate states S_n ($n = 0-4$) during water oxidation. Reprinted with permission from ref. 19. Copyright 2021 American Chemical Society.

has not been determined at present. Based on these latest results, it is strongly believed that one oxygen atom in O_2 comes from the O(5) atom of the Mn_4CaO_5 cluster, and the other oxygen atom comes from the water molecules entering through the surrounding channels.^[23]

n MANGANESE-BASED HETEROGENEOUS ELECTROCATALYSTS

Finding a suitable descriptor is one important direction for the rational design of high-efficient catalysts. With the development of various water oxidation electrocatalysts, various descriptors based on experiments or calculations have been proposed.^[24] The adsorption energy of catalytic intermediates is the most representative descriptor in recent years, which indicates that the adsorption for the reaction intermediates should neither be too strong nor too weak. To simplify the water oxidation reaction step from the perspective of electron transfer, four surface intermediate species could be considered ($^*\text{OH}_2$, $^*\text{OH}$, $^*\text{O}$ and $^*\text{OOH}$). The adsorption of these reaction intermediates can be linked together by a linear proportional relationship, because all reaction intermediates are bound to the surface of the heterogeneous catalyst through O atoms. According to the linear scale relationship, the catalytic activity can be expressed as a volcanic relationship with a single adsorption energy as a descriptor.^[25] However, studies have shown that this adsorption-energy based volcano approach is not well suitable for predicting the catalytic activity of Mn-based materials. According to the existing reports, there is a big difference between the calculated prediction and experimental results.^[26-29] Only considering the method based on adsorption energy is not enough to understand the activity origin of Mn-based catalysts. Therefore, it is necessary to understand the activity origin of Mn-based materials to characterize the exact structural properties and chemical states of these materials through experiments, and link them with catalytic activity. In the following section, we will introduce several Mn-based materials and discuss their structural properties and water oxidation mechanism.

Mn Oxide-based Heterogeneous Electrocatalysts. Since manganese oxide was found to have high catalytic activity under

alkaline conditions, the study of electrocatalytic water oxidation behavior of Mn-based materials has been widely concerned by researchers.^[30-33] Some early reports indicated that Mn-based heterogeneous catalysts have high potential in water oxidation reaction, however the origin of activity was not discussed in detail. Through the synthesis of various Mn oxide materials as a comparative study of model systems, it can simply and clearly reveal the active structural motif. For example, Suib's group prepared manganese oxides of different structures (a-, b-, δ - MnO_2 and amorphous manganese oxide) (Figure 2a), and systematically studied the samples to determine their catalytic activities at high current density under alkaline conditions.^[34] Surprisingly, the experimental results show that the catalytic activity strongly depends on the crystallographic structures and exhibits the following order: a- MnO_2 > amorphous manganese oxide > b- MnO_2 > δ - MnO_2 . Notably, a- MnO_2 has the highest activity (the overpotential is 490 mV under 10 $\text{mA}\cdot\text{cm}^{-2}$, 0.1 M KOH electrolyte, amorphous manganese oxide (590 mV), b- MnO_2 (600 mV), δ - MnO_2 (740 mV)). They suggested that the high activity is due to the following aspect: a- MnO_2 has a mixed oxidation state, unique tunnel structure and abundant protonation sites. These results indicate that the pore structure of materials may be an important factor affecting the catalytic activity, because ion transport becomes more important at higher current density. Our group also systematically studied the unusual hexagonal $\text{Mn}(\text{OH})\text{F}$ rings^[35] and the unusual network of α - MnO_2 nanowires^[36] with structure-induced hydrophilicity and conductivity. It is systematically studied that the high porosity of the 3D superstructure can improve the substrate diffusion efficiency and the unique network structure brings high hydrophilicity and conductivity to enhance the catalytic performance.

Dismukes's team studied the geometric effect of $\text{Mn}(\text{III})\text{O}_6$ octahedrons on electrocatalytic water oxidation.^[37] Through comparative study of g- MnOOH , Mn_2O_3 , b- MnO_2 , δ - MnO_2 and Mn_3O_4 crystalline manganese oxide, it is found that the D_{3d} symmetrical triangular anti-prism $\text{Mn}(\text{III})\text{O}_6$ of Mn_2O_3 exhibits higher water oxidation reaction activity. The reason for the higher water oxidation activity of Mn_2O_3 may also be due to its higher Mn(III) content.^[38] And the tetragonal twisted $\text{Mn}(\text{III})\text{O}_6$ with D_{4h} symmetry of

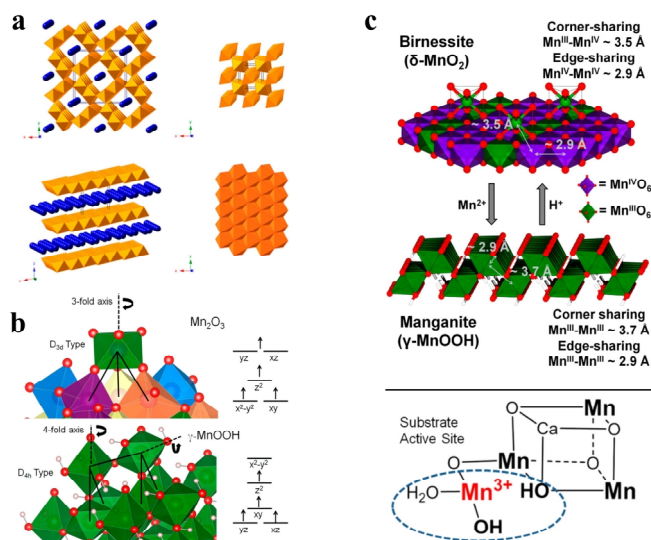


Figure 2. (a) Structures of Mn oxides: α -MnO₂ (2 × 2 tunnel), β -MnO₂ (1 × 1 tunnel), δ -MnO₂ (layered), and amorphous manganese oxides (AMO). Reprinted with permission from ref. 34. Copyright 2014 American Chemical Society. (b) Demonstration of the crystal structure and d-orbital electronic configuration of Mn₂O₃ and γ -MnOOH. (c) Description of corner-shared Mn(III) octahedra in δ -MnO₂ (top) and the biological Mn₄CaO_x cluster (bottom). Reprinted with permission from ref. 37. Copyright 2016 American Chemical Society.

γ -MnOOH shows moderate activity. And β -MnO₂ shows poor catalytic activity. Most notably, the catalytic activity of hexagonal polymorph δ -MnO₂ (HexBir) is much higher than the triclinic polymorph of δ -MnO₂ (TriBir). By comparing the structural characteristics, it can be found that the hexagonal polymorph δ -MnO₂ (HexBir) has some corner-sharing Mn(III)O₆ structure, which is the reason for its excellent catalytic performance (Figure 2c). Through correlation with the high catalytic activity of γ -MnOOH, they further perceived the importance of the corner-sharing Mn(III) content in δ -MnO₂, rather than the total content of Mn(III). In addition, the author further explored the similarity between the corner-sharing Mn(III) species structure in the synthetic catalyst and the dangling Mn(III) of the biological OEC (Figure 2c, bottom). They believe that the active site structure and electronic structure of synthetic artificial catalysts similar to those of biological OEC are the reason of their high catalytic activity.

The geometry of Mn(III) octahedra was studied in greater detail by comparing γ -MnOOH and Mn₂O₃ which contain only Mn(III) species. As shown in Figure 2b, γ -MnOOH only contains the Mn(III)O₆ type structure of Mn(III) in its unit cell. This configuration is affected by the Jahn-Teller distortion to form a tetragonal elongation (D_{4h} type) octahedron. This distortion causes each D_{4h} type octahedron to form four short and two long Mn–O bonds, and individual D_{4h} units are connected to three other Mn(III)O₆ octahedra by corner-sharing bridges. In contrast, Mn₂O₃ contains five symmetric non-equivalent Mn(III)O₆ sites in its unit cell. In three of the five sites, due to the distortion of the D_{4h} symmetry, all Mn–O bonds have different lengths, with two long and four

short. In the other two sites, all bond lengths are very similar, indicating D_{3d} symmetry of the triangular anti-prism. The sites are connected to another two or three Mn(III)O₆ by corner sharing bridges, and thus these sites can be compared with the typical γ -MnOOH. The surface of Mn(III)O₆ is located above the three-fold axis and maintains the D_{3d} symmetry formed by three oxo bridges. Therefore, there is an e_g¹ electronic configuration. Since the triangular ligand field of the fixed oxo bridge suppresses the Jahn-Teller distortion of the quadrilateral, the Mn–O bond length is expected to be almost equal. The three surface-bound water-oxidizing oxygen sites are considered to be relatively flexible, which could be beneficial to catalytic activity if the oxygen release from this site is rate-limiting.

Nocera's research team conducted a detailed study on a disordered δ -MnO₂ catalyst system.^[39] They found that the enhancement of catalytic activity began with a structural phase transformation through the charge comproportionation of the original δ -MnO₂ film with generated Mn(OH)₂ to produce a Mn₃O₄-like intermediate structure (δ -Mn(IV)O₂ + 2Mn(II)(OH)₂ → Mn(II,III)₃O₄ + 2H₂O). The continuous anode potential further oxidizes the Mn₃O₄-like intermediate structure into disordered δ -MnO₂. In addition, in-situ XAS measurement results show that Mn(III) groups still exist in the catalyst during the water oxidation reaction but with a lower coordination number. The coordination number of Mn–O is reduced to four, and the bond length is relatively stable, indicating that Mn(III) may cooperate with a tetrahedral coordination field. The tetrahedral ligand field of Mn(III) inhibits further oxidation and the valence state is still trapped at Mn(III) even at a high applied anode potential. The researchers proposed a unique structural motif of the tetrahedral Mn(III) intermediate species in the disordered δ -MnO₂ located next to the Mn(IV)O₆ octahedron. The calculation of the electronic structure of this unique local coordination structure motif shows that the reconstruction of Mn 3d and O 2p states contributes to the formation of oxygen holes. In other words, the trapped Mn(III) species in the tetrahedral ligand field cause local strain to distort the Mn–O coordination bond nearby, resulting in a narrower gap between the highest occupied and lowest unoccupied orbitals of the oxygen radical. Therefore, they believe that this unique local structure in the disordered MnO₂ facilitates the generation of highly active Mn-oxyl radical species, thereby enhancing the electrochemical catalytic activity.

Mn Phosphate-based Heterogeneous Electrocatalysts. According to previous studies, it is found that Mn(III) is an important active intermediate in Mn-based catalysts.^[29,39–42] In a neutral solution, the Mn(III) intermediate will undergo a disproportionation reaction to form Mn(II) and Mn(IV) species, making Mn(III) unable to exist.^[43–45] In order to solve this problem, a large number of asymmetric structures are introduced into the Mn geometry. The asymmetry in the crystal frameworks can tolerate J-T distortion and thereby stabilize the Mn(III) intermediate.^[46] Although transition metal phosphate compounds have been widely investigated as cathode materials for lithium-ion batteries, there have been few attempts to study the OER catalytic performance of phosphate-containing manganese-based crystals.^[47] In this

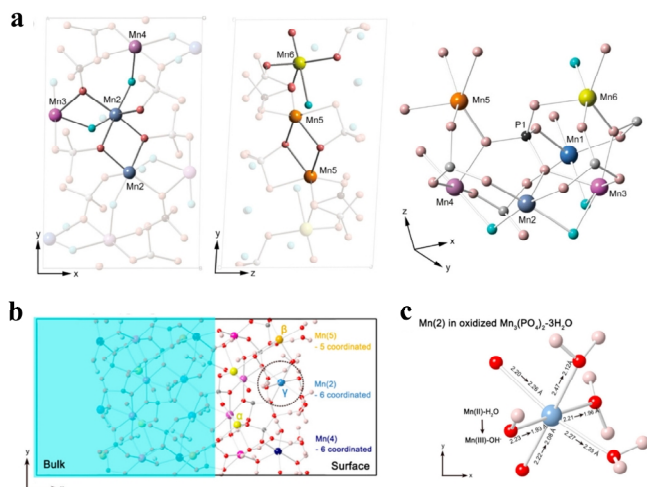


Figure 3. (a) Structure of $\text{Mn}_3(\text{PO}_4)_2 \cdot 3\text{H}_2\text{O}$. (b) (100) Surface structure of $\text{Mn}_3(\text{PO}_4)_2 \cdot 3\text{H}_2\text{O}$. (c) Bonding geometry of the J-T distorted surface Mn(2) atom of oxidized manganese phosphate, in which some Mn(II) atoms were intentionally oxidized to Mn(III). Reprinted with permission from ref. 48. Copyright 2014 American Chemical Society.

chapter, we will introduce several Mn-based phosphate materials and discuss their asymmetric structures.

The hydrated Mn(II) phosphate ($\text{Mn}_3(\text{PO}_4)_2 \cdot 3\text{H}_2\text{O}$) as a water oxidation catalyst was investigated by Nam et al.^[48] They synthesized a new crystal structure as water oxidation catalyst and identified the OER catalytic activity under neutral conditions (the overpotential is 680 mV under $0.1 \text{ mA} \cdot \text{cm}^{-2}$, 0.5 M phosphate buffer at pH = 7.0). They verified that the bulky phosphate polyhedron induces a less-ordered Mn geometry in $\text{Mn}_3(\text{PO}_4)_2 \cdot 3\text{H}_2\text{O}$, and its structure is similar to that of catalytic active Mn(III)-containing materials. Computational analysis revealed that distinctive structural features of $\text{Mn}_3(\text{PO}_4)_2 \cdot 3\text{H}_2\text{O}$ could successfully stabilize Mn(III) during water oxidation, leading to superior catalytic activity under neutral conditions. In detail, they first focused on the crystal structure of $\text{Mn}_3(\text{PO}_4)_2 \cdot 3\text{H}_2\text{O}$. As shown in Figure 3a, Mn(2) atoms are connected to each other by edge O–O sharing. The Mn(2) and Mn(3) atoms are bridged by edge O– O_w (oxygen atom in a water molecule) sharing, and the Mn(2) atoms are linked to Mn(4) atoms by O_w vertex sharing. The Mn(5) atoms share two oxygen atoms with each other, forming Mn_2O_8 dimers. The Mn(6) atom does not share any atoms with other manganese atoms. Spherical cluster around the P(1) site illustrates the asymmetrical arrangement of manganese atoms in the crystal. Because crystal structure is considered to be one of the major sources of catalytic capacity, especially for Mn containing catalysts, the stabilization of Mn(III) in the OER process and the initial content of Mn(III) in the crystal structure are very important, as evident in OEC and Mn_2O_3 .^[41] They observe the effect of the oxidation of Mn(II) ions inside the catalyst to Mn(III) on the crystal structure by calculation and simulation. Calculations show that there is a certain degree of J-T distortion in $\text{Mn}_3(\text{PO}_4)_2 \cdot 3\text{H}_2\text{O}$ to stabilize Mn(III). At the same time, the average pressure when all Mn atoms are in the Mn(III) configuration is measured to measure the stability of Mn(III). When Mn(III) atoms are abundant,

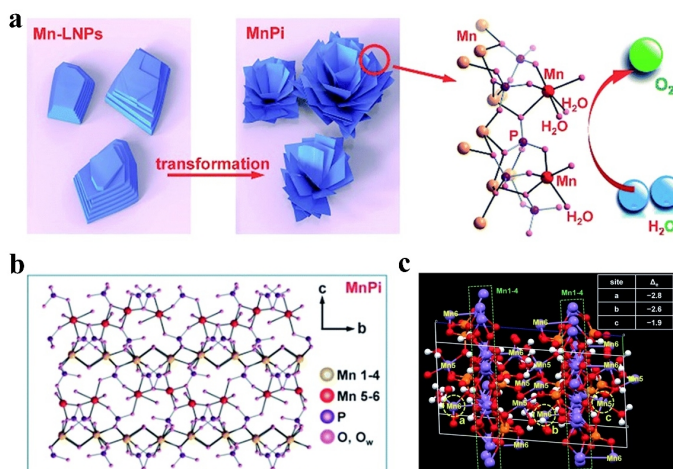


Figure 4. (a) Ultrathin MnPi nanosheet assembly with native asymmetric out-of-plane Mn centers (red) derived from the transformation of layered phosphates for electrocatalytic water oxidation. (b) The crystal structure of MnPi with six different Mn sites, including Mn(1-4) layers and out-of-plane Mn(5,6) centers. (c) The unit cell of MnPi used to calculate the preference of the oxidation of different Mn sites. The three Mn sites that can be most easily oxidized are marked with yellow circles. Reprinted with permission from ref. 50. Copyright 2018 Royal Society of Chemistry.

greater pressure means the tendency of lattice distortion and instability. The magnitude of pressure follows the order $\text{MnO}_2 > \text{MnO} > \text{Mn}_3(\text{PO}_4)_2 \cdot 3\text{H}_2\text{O}$. Therefore, they conclude that the structural elasticity of the stable Mn(III) state could explain the high catalytic activity of $\text{Mn}_3(\text{PO}_4)_2 \cdot 3\text{H}_2\text{O}$. On the surface of the terminal body, the exposed Mn(2), Mn(4) and Mn(5) atoms are 6-, 6- and 5-coordination, respectively (Figure 3b). In order to compare the activity of Mn ions on each surface, they were taking electrons one by one from the system and relaxing the structure. The results show that 5-fold Mn atoms have stronger catalytic activity than the 6-fold Mn ones. In addition, due to the presence of PO_4 dangling bonds near the Mn atom, some Mn(II)– H_2O bonds are found on the surface and underground to transfer hydrogen to the dangling bonds, resulting in Mn(III)–OH (Figure 3c). In fact, the phosphate group can participate in PCET as a proton acceptor in the OER catalysis process.^[49] Although whether the catalyst follows the PCET reaction in the OER catalysis process requires more experimental evidence, they thought that phosphate ions can promote the PCET reaction to oxidize the Mn–OH₂ center according to the calculation results. Therefore, in addition to the structural flexibility facilitating the J-T distortion and the 5-fold Mn(II) atoms that are more conducive to oxidation than the 6-fold Mn(II), the surface catalytic effect increases owing to the PO_4 dangling bonds near the Mn atoms.

The direct relationship between the asymmetric structures in manganese-based catalysts and their electrocatalytic activity for water oxidation reaction was also supported by our group. We report a manganese(II) phosphate nanosheet assembly with asymmetric out-of-plane Mn centers from the transformation of amine-intercalated nanoplates for efficient electrocatalytic water oxidation in neutral aqueous solutions (the overpotential is 563

mV under $1 \text{ mA} \cdot \text{cm}^{-2}$, 0.05 M phosphate buffer at $\text{pH} = 7.0$) (Figure 4a).^[50] The crystal structure of the MnPi is illustrated in Figure 4b. This structure contains six different Mn sites (Mn(1), Mn(2), Mn(3), Mn(4), Mn(5) and Mn(6)). First, 6-coordinated Mn(1), Mn(2), Mn(3) and Mn(4) octahedrons are connected on the a-b axis to form a dense layer parallel to the (001) plane. Then, the 5-coordinate Mn(5) triangular bipyramid and 6-coordinate Mn(6) octahedron are located outside the (001) plane to form another layer. It can be noted that Mn(5) and Mn(6) have one and two terminal coordinated water molecules, respectively. The terminal water on Mn(5,6) can participate in water oxidation to form O_2 . After O_2 is released, these coordination sites will be used by new water molecules. In MnPi, the Mn(5) trigonal bipyramid is highly distorted with one terminal water-coordination. This structure is essentially promising for water oxidation. And Mn(5) is 5-coordinated, which has the highest tolerance to Mn(III) distortion. The first-principles density functional theory (DFT) calculations were performed to determine the active Mn center in MnPi. The charge difference on the Mn atoms is simulated and calculated. In Figure 4c, the top three Mn sites with the largest reduction valence charge are marked with yellow circles. Two of them are the 6-coordinated Mn(6) sites with two terminal water molecules, and the remaining one is the 5-coordinated Mn(5) site with one terminal water molecule. The coordinated terminal water molecules further promote the oxidation of the corresponding Mn center by providing a disposable proton. In summary, the advantages of Mn(5) and Mn(6) centers are mainly to coordinate with the terminal water molecules to provide vacancies for OER substances. They are also considered as the out-of-plane Mn centers, which is similar to that of the dangling Mn4 (Figure 1b) in the Mn cluster in OEC. And they can be oxidized at a low potential to form intermediate state Mn(III).

On the basis of the previous work, the relationship between the amount of Mn(III) in Mn-based phosphate catalysts and their electrocatalytic activity for the water oxidation was further supported by our group.^[51] We reported two autologous phosphates ($\text{Mn}_2\text{P}_2\text{O}_7$ and $\text{Mn}_3(\text{PO}_4)_2$, the overpotentials are 555 and 630 mV under $1 \text{ mA} \cdot \text{cm}^{-2}$, 0.05 M phosphate buffer at $\text{pH} = 7.0$) obtained from the same parent material for electrocatalytic water oxidation. The two autologous materials have similar morphology, crystallinity and surface areas, which make them a good platform for studying water oxidation in response to the Mn coordination environment. Both materials have monoclinic structures. In $\text{Mn}_2\text{P}_2\text{O}_7$, there is only one type of 6-coordinated Mn(II) center. And there are three types of Mn(II) centers in the $\text{Mn}_3(\text{PO}_4)_2$ crystal. One is the 6-coordinated (Mn(1)) octahedron and the other is the 5-coordinated (Mn(2), Mn(3)) trigonal bipyramid. The electrocatalytic water oxidation of the synthesized manganese phosphates was studied in 0.05 M phosphate buffer ($\text{pH} = 7.0$) by cyclic voltammetry (CV), and the catalytic performance of $\text{Mn}_2\text{P}_2\text{O}_7$ is better than that of $\text{Mn}_3(\text{PO}_4)_2$ with the same Mn valence. The presence of Mn(III) intermediate in $\text{Mn}_2\text{P}_2\text{O}_7$ and $\text{Mn}_3(\text{PO}_4)_2$ catalysts during electrolysis is identified by the determination of the Mn(III)-pyrophosphate (pp) complex, which has a characteristic ligand-to-metal charge transfer (LMCT) absorption at 258 nm .^[52,53] In contrast, the relative absorption of

$\text{Mn}_2\text{P}_2\text{O}_7$ catalyst solution is very obvious, indicating that the structure can provide more amount Mn(III). According to the electrochemical and spectroscopic results, it has been straightforwardly observed that highly asymmetric geometry of $\text{Mn}_2\text{P}_2\text{O}_7$ can stabilize the active Mn(III) with J-T distortion and form abundant active centers. In addition to stabilize the central manganese structure, phosphate can also form a rich, extensive and continuous hydrogen bond network to accelerate the proton transfer rate, which further promotes the electrocatalytic water oxidation.^[54]

Mn-based Heterogeneous Electrocatalysts with Heteroatom Incorporation. Introducing heteroatoms into Mn-based materials is also one of the hotspots of research in recent years, although it is difficult to fully understand the exact role of each element.^[55–58] Nam's group selected the pyrophosphate-based Mn compound $\text{Li}_2\text{MnP}_2\text{O}_7$ as a model system and investigated the role of the Mn valence in the catalytic activity (LiMnP_2O_7 , 5.0 A/g at an overpotential value of 680 mV in 0.5 M phosphate buffer at $\text{pH} = 7.0$).^[43] By controlling the content of lithium, the valence of Mn in the material is changed (Figure 5a). The XANES spectrum of Mn K-edge shows that the average oxidation state of Mn increases as the Li content decreases (Figure 5c). The catalytic current density and exchange current density increased proportionally with the amount of Mn(III) species, while the Tafel slopes are similar, indicating that the number of active sites of catalyst is directly related to the Mn(III) species (Figure 5b). In addition, the

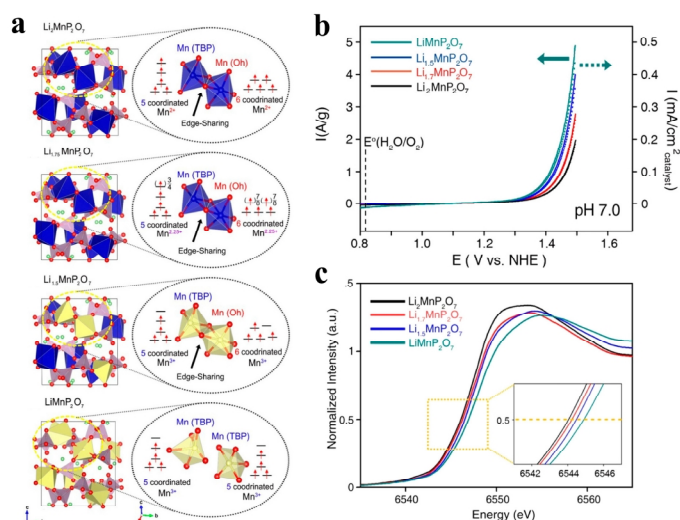


Figure 5. (a) Simulated crystal structures of the $\text{Li}_2\text{MnP}_2\text{O}_7$, $\text{Li}_{1.75}\text{MnP}_2\text{O}_7$, $\text{Li}_{1.5}\text{MnP}_2\text{O}_7$ and LiMnP_2O_7 unit cells. The inset shows the local Mn environment around the Mn_2O_9 subunit. Mn^{2+} and Mn^{3+} atoms in the unit cell are shown in blue and yellow, respectively. (b) Polarization-corrected cyclic voltammetry curves of LiMnP_2O_7 (green), $\text{Li}_{1.5}\text{MnP}_2\text{O}_7$ (blue), $\text{Li}_{1.7}\text{MnP}_2\text{O}_7$ (red) and $\text{Li}_2\text{MnP}_2\text{O}_7$ (black) in 0.5 M sodium phosphate buffer ($\text{pH} 7.0$). (c) XANES Mn K-edge spectra of $\text{Li}_{2-x}\text{MnP}_2\text{O}_7$ ($x = 0, 0.3, 0.5, 1$) powders. The inset shows the average oxidation state of Mn atoms gradually changes. Reprinted with permission from ref. 43. Copyright 2014 American Chemical Society.

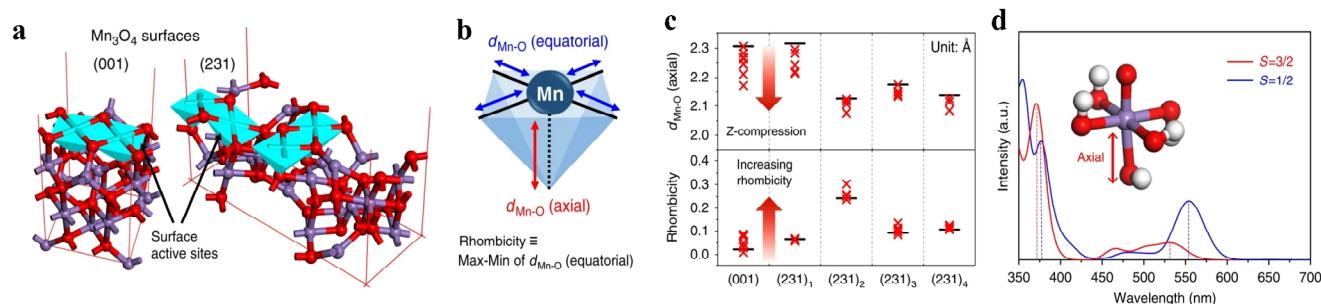


Figure 6. DFT calculations to evaluate the impact of Ni substitution in Mn oxide. (a) The (001) and (231) surface structures of Mn_3O_4 . (b) Schematic illustration of the surface Mn active site. (c) The impact of Ni substitution on the axial Mn–O distance and rhombicity of equatorial Mn–O distances of the Mn_3O_4 (001) and (231) surface active sites. (d) The UV-Vis spectra of the high-spin and low-spin Mn(IV) site cluster models. Reprinted with permission from ref. 59. Copyright 2020 Nature Publishing Group.

Baur distortion index is also calculated, which can reflect the degree of asymmetry of the local Mn octahedron. Interestingly, the catalytic activity and Baur distortion index showed similar linear dependence on the amount of Mn(III) species, which means the amount of Mn(III) species and asymmetric local coordination of Mn are directly related to the activity of Mn-based heterogeneous catalysts in electrochemical water oxidation.

Furthermore, they reported the spectroscopic characterization of new intermediates during the water oxidation reaction of Mn-based heterogeneous catalysts and assigned them as low-spin Mn(IV)-oxo species (Figure 6).^[59] It shows that the engineering of the local distortions via Ni atom substitution in Mn_3O_4 NPs manipulates the spin state of the reaction intermediates during water oxidation reaction (Ni- Mn_3O_4 NPs/NiO, the overpo-

tential is 420 mV under $1 \text{ mA} \cdot \text{cm}^{-2}$, 0.5 M phosphate buffer at pH = 7.0). Through a combination of experiment and computation, they explored the effect of Ni atom substitution on the intermediate species of nanoscale manganese oxide NPs, and found that the Ni substitution enables the compression of surface Mn octahedron, thereby producing low-spin Mn(IV)-oxo intermediate species in the water oxidation reaction.

So far, two widely accepted OER mechanisms include adsorbate evolution mechanism and lattice oxygen oxidation mechanism.^[60,61] No matter which OER mechanism the catalyst surface follows, the formation of O–O bond can follow two different ways, acid-base nucleophilic attack and direct radical coupling.^[61,62] For acid-base nucleophilic attack pathway, there is an inherent linear scaling relation (LSR) between the adsorption

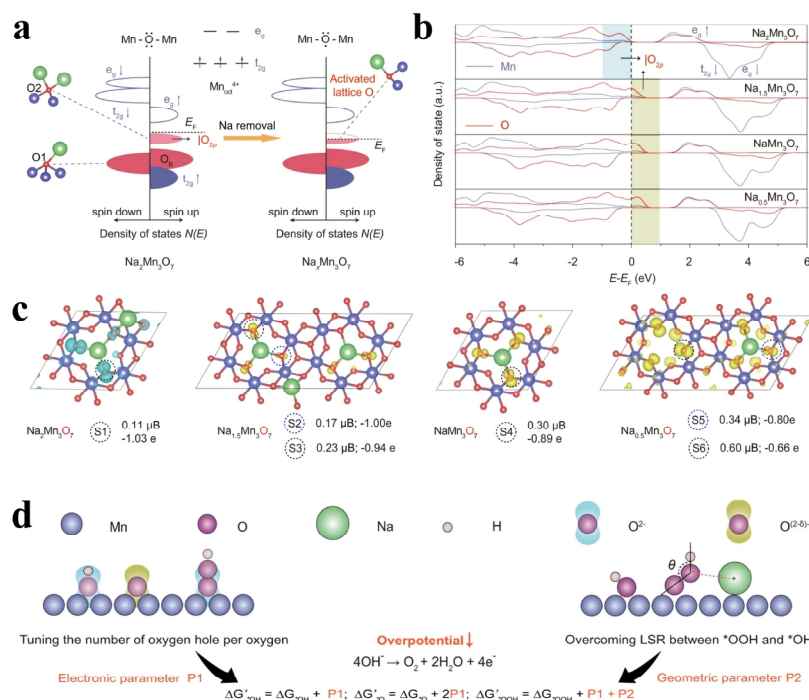


Figure 7. (a) Schematic formation of oxygen holes in $|\text{O}_{2p}$ lone-pair states for $\text{Na}_x\text{Mn}_3\text{O}_7$. (b) Projected density of states of $\text{Na}_x\text{Mn}_3\text{O}_7$ slabs ($x = 2, 1.5, 1$ and 0.5). (c) Partial charge density projected on O atoms by the shaded region shown in Figure 7b. (d) Scheme of rational design of better $\text{Na}_x\text{Mn}_3\text{O}_7$ electrocatalysts. Reprinted with permission from ref. 64. Copyright 2021 Nature Publishing Group.

energy of $^*\text{OOH}$ and $^*\text{OH}$ intermediates. The inherent LSR for most catalytic materials imposes a theoretical overpotential ceiling, limiting the development of efficient electrocatalysts.^[60,63] Therefore, current research efforts are mainly directed to overcome the limitation from such LSR for developing practical electrocatalysts. Wang's group used $\text{Na}_x\text{Mn}_3\text{O}_7$ with adjustable amount of Na^+ as model to unlock the specific coordination configuration that can regulate the barrier symmetry between O–H bond cleavage and $^*\text{OOH}$ formation on the basis of overcoming the LSR between $^*\text{OOH}$ and $^*\text{OH}$ (Figure 7).^[64] Through a combination of in-situ spectroscopy-based characterization and first-principles calculations, they revealed that the number of Na^+ is critical to the overall activity improvement. In terms of electronic effect, the O–O bond formation is promoted as the number of Na^+ reduces, because of the increased number of oxygen holes in $|\text{O}_{2p}$ upon activating lattice oxygen, and the relative barrier between O–H bond cleavage and O–O bond formation is regulated. In terms of geometric effect, the overpotential ceiling increases as the number of Na^+ reduces due to the weakening of Na^+ -specific stabilizing effect on the pendant oxygen in $^*\text{OOH}$. As a result of the above two opposite effects, an intermediate level of Na^+ mediation (NaMn_3O_7) exhibits the optimum OER activity (NaMn_3O_7 , the overpotential is 280 mV under 0.25 $\text{mA}\cdot\text{cm}^{-2}$ in O_2 -saturated 1 M KOH electrolytes at pH = 13.8). In addition, the oxygen precipitation mechanism and active site were verified. Resolving the near-surface structures under electrochemical condition of the catalyst is a prerequisite for understanding the OER mechanism and related active site. The in-situ X-ray photoelectron spectroscopy (XPS) measurements were performed on NaMn_3O_7 . The pH-dependent experiment and Raman spectra further demonstrate it works in a decoupled proton/electron route with the presence of negatively charged oxidized oxygen species. By combining all results, they demonstrate that the activation of lattice oxygen leads to the enhanced OER activity, as the Fermi level enters the $|\text{O}_{2p}$ states for $\text{Na}_x\text{Mn}_3\text{O}_7$ ($x < 2$) due to the charge compensation and redistribution, creating the reactive oxygen radicals on the surface which behave as electrophilic centers prone to nucleophilic attack from the oxygen lone pairs of OH^- . This work provides a guideline for the development of better catalysts towards water oxidation or other oxidative reactions through tuning both lattice oxygen reactivity and scaling relation.

n WATER OXIDATION MECHANISM OF Mn-BASED HETEROGENEOUS ELECTRO-CATALYSTS

In addition to the knowledge of constructing stable intermediate states with different structures discussed, exploring the entire mechanism cycle and determining the slowest step are very important to further understand the OER mechanism of Mn-based catalysts. We first describe the basic steps of the electrochemical water oxidation reaction and explain the concept of rate-determining steps (RDS). Next, we summarized the reaction mechanisms of several representative Mn-based catalysts.

The Basic Steps and Rate-determining Steps of Electrochemical Water Oxidation. Electrochemical water oxidation to

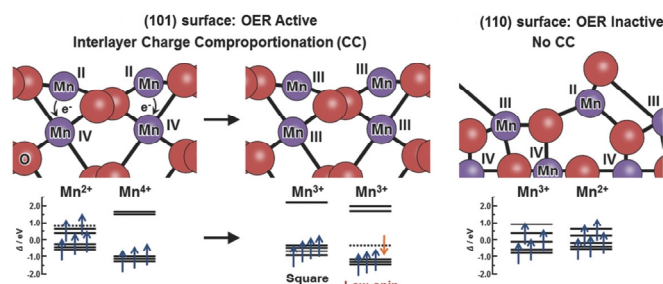


Figure 8. Schematic image of surface valency changes on (101) and (110) surfaces of $\beta\text{-MnO}_2$ after the reduction of surface Mn atoms. Reprinted with permission from ref. 68. Copyright 2018 John Wiley and Sons.

O_2 is a multi-step reaction involving transfer of four electrons and four protons, including electrochemical steps and chemical steps. Electrochemical steps involve PCET, which includes both electron transfer (ET) and proton transfer (PT); the chemical steps mainly include the formation of O–O bonds, the release of O_2 and the charge rearrangement of catalyst materials.^[65,66] The oxidizing power accumulates on the catalyst material to form high-valent active intermediate species in the electrochemical oxidation steps before the O–O bond formation step.^[67] First, the PCET process could be carried out in two ways: stepwise sequential electron and proton transfer (PT-ET or ET-PT) or concerted proton and electron transfer. During the electrochemical oxidation process, different intermediate species could be formed and some are unstable with charge rearrangement occurring rapidly, thereby reducing the concentration of active intermediate species. For example, the charge rearrangement of Mn(III) is closely related to the reaction conditions such as pH and the surface structure of the catalyst material.^[68] The charge disproportionation of Mn(III) in $\delta\text{-MnO}_2$ is a representative example of a charge rearrangement process (Figure 8). And Mn(III) species is 11-fold higher on (101) surfaces compared with on the (110) surfaces in $\beta\text{-MnO}_2$ because Mn(III) species are favorably generated by the charge ratio between the layers of Mn(II) and Mn(IV) on the (101) plane. Therefore, it is important to explore the stability of the intermediate. For biological OEC, the O–O bond formation step in the OER process is still unknown. The formation of O–O bond can follow two different ways, acid-base nucleophilic attack and direct radical coupling. In the former case, a substrate water molecule or hydroxide ion nucleophilically attacks the high-valent metal-oxo/oxyl species and is deprotonated to generate a hydroperoxo intermediate, while in the latter case, two high-valent metal-oxo/oxyl species directly couple with each other to form a bridging peroxo intermediate. For example, Spiccia's research team studied the O–O bond formation pathway on a Ca decorated $\delta\text{-MnO}_2$ catalyst, including both acid-base nucleophilic attack and direct radical coupling.^[69]

The total reaction rate is usually determined by the elementary step with the slowest reaction rate. This slowest step is known as the RDS. Due to the different types of catalysts and reaction conditions, both electrochemical and chemical steps may become RDS. The Tafel slope observed in the electrochemical

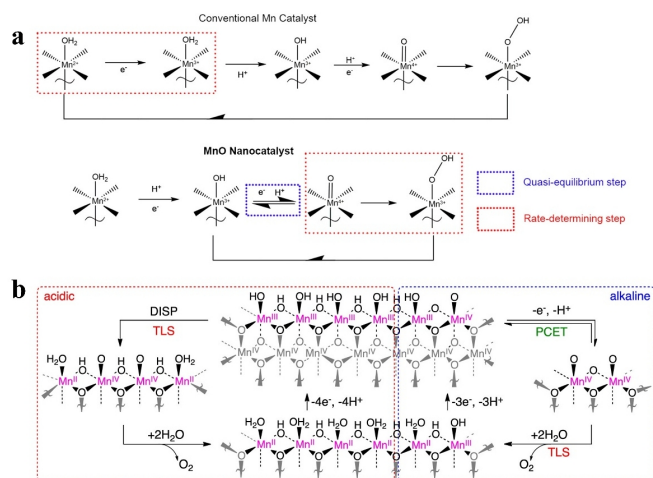


Figure 9. (a) Suggested mechanism of manganese oxide nanoparticles for water oxidation. Reprinted with permission from ref. 68. Copyright 2017 American Chemical Society. (b) Proposed mechanism for the OER on MnO_x in (left) acidic and (right) alkaline conditions. Reprinted with permission from ref. 71. Copyright 2014 American Chemical Society.

kinetic experiments provides information on the catalytic activity and RDS. Besides, the reaction-order analysis, such as pH or concentration dependence, can help to identify RDS by prompting whether there are protons or electrolytes involved in RDS. Combining RDS obtained by electrochemical kinetic analysis and in-situ spectroscopy to determine the information of active intermediates can provide a more comprehensive understanding of the reaction mechanism.

Mechanism Cycle of Mn-Based Heterogeneous Electrocatalyst for Water Oxidation. According to the number of Mn atoms constituting the active site, the proposed mechanisms can be divided into two categories. The first is the monomeric active site. The manganese undergoes sequential oxidation steps to form the high-valent Mn-oxo species before O–O bond formation via the acid-base nucleophilic attack pathway. The second is the multimetric active site. It is particularly important to understand the charge rearrangement processes between the manganese atoms. Highly active Mn-oxyl species are formed through oxygen-centered oxidation and O–O bond formation proceeds via the direct radical coupling pathway.^[67]

Based on both electrochemical kinetic analysis and various spectroscopic results, an overall water oxidation mechanistic scheme was constructed for Mn species on the nanoparticle surface. Nam's group proposed that monomeric Mn(IV)=O species were responsible for the slowest O–O bond formation step through acid-base nucleophilic attack pathway after generation through the PCET of Mn(II)-OH₂ and Mn(III)-OH species (Figure 9a).^[68] The RDS change from a charge accumulation step to the O–O bond formation step also corresponds well with the experimental results reported by Dau's group,^[70] which verified the stable charge accumulation of oxidizing power through the fast Mn-centered redox-state change (Mn(III)-Mn(IV)) in catalytically active manganese oxides. Nocera's group performed electro-

chemical kinetic analysis of layered manganese oxide (δ -MnO₂) over the entire pH range (Figure 9b).^[71] Tafel and reaction order analyses were performed by measuring the current-voltage, phosphate concentration-dependent current density and pH-dependent current density characteristics of the catalyst. Under alkaline conditions, they suggested that the surface of the catalyst consisted of a mixture of Mn(III) and Mn(IV) valence states. They suggested that Mn(III)-OH is converted to Mn(IV)=O via a PCET pre-equilibrium step before the O–O bond formation through the direct coupling as the RDS. Under acidic conditions, based on previously observed unstable Mn(III) species on the surface of δ -MnO₂ below pH 9.0, they assigned that the cross-site proton coupled charge disproportionation of Mn(III) is RDS. Four Mn(III)-OH species disproportionated to give two Mn(II)-OH₂ and two Mn(IV)=O; and the adjacent Mn(IV)=O then coupled to form the O–O bond. The low catalytic activity of δ -MnO₂ under acidic conditions originated from the small proportion of four adjacent Mn(III)-OH species on the catalyst surface. At near-neutral pH, they proposed that the reaction mechanism of δ -MnO₂ was a mixture of the two competing pathways presented above rather than one specific mechanism.

Recent reports proposed interesting hypothetical water oxidation pathways that involve high-valent Mn species. Naruta and Zahran suggested that Mn(V)=O is a highly active species of the catalyst. When the electrolyte was changed from aqueous phosphate buffer to a non-aqueous solution, the RDS changed from ET to the O–O bond formation chemical step.^[72] Combined with the results of electrochemical kinetic analysis and kinetic isotope effect experiment, they suggested that Mn(V)=O is generated via the sequential oxidation steps of Mn(II)-OH₂ → Mn(III)-OH → Mn(IV)=O → Mn(V)=O and is the active species for the RDS of O–O bond formation by the acid-base nucleophilic attack pathway in non-aqueous electrolyte solution. Sun's group prepared c -disordered δ -MnO₂ by annealing electrodeposited manganese oxides, then got their electrochemical kinetic parameters.^[42] However, the RDS remained unclear because of the difficulty of interpreting the derived species originating from the strong interactions between various redox sites. They performed ex-situ infrared spectroscopy and detected the intermediate species of Mn(VII)=O, believing that at least four Mn sites are involved in the oxidation reaction of water, and the Mn(VII)=O intermediate is generated through charge rearrangement.

Mechanism Cycle of Mn-based Homogeneous Electrocatalyst for Water Oxidation. Compared with material catalysts, the structures of molecular catalysts are clearer. The structure-function relationships of molecular catalysts can be systematically studied.^[73-76] For O–O bond formation step, three different possibilities have been discussed (Figure 10a): (1) an acid-base (AB) mechanism involving the nucleophilic attack of water or hydroxide on a formal Mn(V)-oxo species, (2) a radical coupling (RC) of two bridging metal-oxo species, or (3) a RC of the dangling Mn(IV)-O[•] radical with a bridging oxygen in the manganese cluster.^[77,78] Despite experimental and theoretical model studies, the actual mechanism for the formation of molecular oxygen at OEC has stayed ambiguous to date. Recently, an excellent sys-

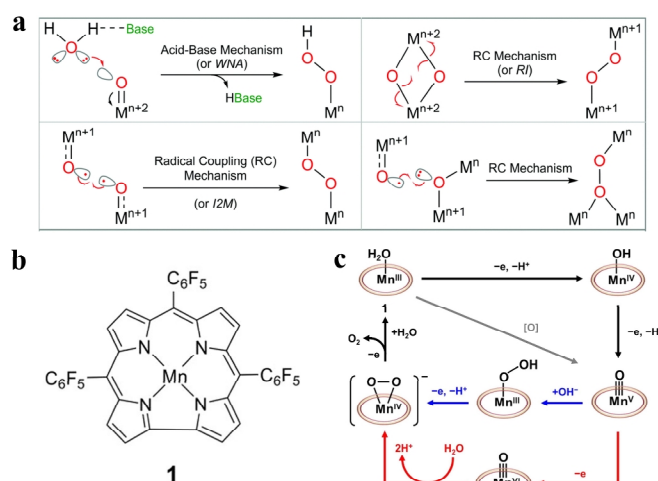


Figure 10. (a) Proposed O–O bond formation mechanisms in chemistry and biology. Reprinted with permission from ref. 78. Copyright 2021 Royal Society of Chemistry. (b) Molecular structure of **1** and (c) Proposed mechanisms for water oxidation with **1**. Reprinted with permission from ref. 79. Copyright 2021 American Chemical Society.

tem is established, in which Mn-oxo has considerable activity for water oxidation and meanwhile has satisfactory stability for characterizations and reactivity studies.^[79] By studying Mn tris(pentafluorophenyl)corrole **1** (Figure 10b), we provided evidence for a Mn-based WNA mechanism. The Mn(IV)-peroxo intermediate was identified by UV-vis spectra, EPR, infrared, high-resolution mass spectrometry and isotope-labeling experiments, confirming the nucleophilic attack of the O–O bond formation mechanism. We identified the formation of Mn(V)(O) at the Mn(V/IV) potential prior to catalyzing water oxidation and Mn(IV)-peroxo at the potential to initiate water oxidation. On the basis of these results, we can propose the mechanism of water oxidation with **1** (Figure 10c). Mn(V)(O) can be generated electrochemically (black line) and chemically (gray line). The reaction of Mn(V)(O) with hydroxide is fast, leading to the formation of the monovalent anion of Mn(III)-OOH, which is then oxidized by unreacted Mn(V)(O) and deprotonated with excess hydroxide to give a Mn(IV)-peroxo species (blue line). However, nucleophilic attack of water on Mn(V)(O) is so extremely slow that further oxidation of Mn(V)(O) is required to become more active to react with water under electrocatalytic conditions, and the formal Mn(VI)(O) describes this 1e[−]-oxidized Mn(V)(O) species. According to calculations, WNA on Mn(VI)(O) is dynamically feasible to generate Mn(IV)-peroxide (red line in Figure 10c), which can then be oxidized or disproportionated to produce O₂ and Mn(III). We also studied WNA on metal-oxo units with similar coordination environments, which suggested a similar WNA mechanism involved in water oxidation.^[80,81]

CONCLUDING REMARKS

The reason why Mn-based heterogeneous catalysts have attracted much attention in water oxidation is mainly that the biological photosystems only use four manganese atoms to achieve the highest turnover frequency. Inspired by natural photosystems,

designing highly efficient, stable, cost-effective and environmentally-friendly electrocatalysts is the goal for efficient water oxidation. However, despite pioneering efforts of many groups in the development of Mn-based heterogeneous catalysts, there are still huge gaps between synthetic catalysts and biological photosystems in terms of performance and understanding of the mechanism at the atomic level. To address this, we thought that it is necessary to summarize the internal structural characteristics of the synthetic catalyst to clarify the specific structural characteristics and whether they are related to the OER process, so as to further understand the OER mechanism. In the water oxidation reaction, the OEC catalyzes water splitting into electrons, protons, and dioxygen through a five-state cycle. The atomic arrangements and oxidation state in every S_n state except the S₄ state have been experimentally revealed. However, we still do not have any direct experimental evidence for the O–O bond formation step in the biological system, even though it is the most important and RDS. In this regard, the investigation of heterogeneous catalysts can provide useful information to understand the mechanism by capturing intermediates and decoupling kinetic parameters.^[82]

In order to better understand the oxidation process of water, the reaction rate constant of each step needs to be measured. However, the complexity of the catalyst surface makes the situation difficult. Furthermore, the fact that electrons are transferred between the catalyst surface and the electrode should always be considered.^[83] In this review, considerable knowledge has been obtained from the analysis of thermodynamically stable crystals of manganese materials, but there is still a lot of room to make metastable phases, especially on the surface of the catalyst. Additionally, we would like to bring attention to the effect of entropy during water oxidation, as proposed recently.^[84] In addition to enthalpy-based methods to control the combination of intermediates on the catalyst surface, the important contribution of entropy mainly involving water molecules needs to be considered. All in all, we hope that the review can provide useful guidance for the future research directions of Mn-based water oxidation catalysts. More exciting science will be revealed in the future, and the input of scientists and engineers in related research fields will be highly needed.

ACKNOWLEDGEMENTS

The project was supported by the Starting Research Funds of Shaanxi Normal University and the National Natural Science Foundation of China (21872092).

AUTHOR INFORMATION

Corresponding authors. Emails: zw@snnu.edu.cn (W.Z.) and ruicao@snnu.edu.cn (R.C.)

COMPETING INTERESTS

The authors declare no competing interests.

ADDITIONAL INFORMATION

Full paper can be accessed via <http://manu30.magtech.com.cn/jghx/EN/10.14102/j.cnki.0254->

5861.2022-0024

For submission: <https://mc03.manuscriptcentral.com/cjsc>

REFERENCES

- (1) Cook, T. R.; Dogutan, D. K.; Reece, S. Y.; Surendranath, Y.; Teets, T. S.; Nocera, D. G. Solar energy supply and storage for the legacy and nonlegacy worlds. *Chem. Rev.* **2010**, 110, 6474–6502.
- (2) Benson, E. E.; Kubiak, C. P.; Sathrum, A. J.; Smieja, J. M. Electrocatalytic and homogeneous approaches to conversion of CO₂ to liquid fuels. *Chem. Soc. Rev.* **2009**, 38, 89–99.
- (3) Turner, J. A. Sustainable hydrogen production. *Science* **2004**, 305, 972–974.
- (4) Marini, S.; Salvi, P.; Nelli, P.; Pesenti, R.; Villa, M.; Berrettoni, M.; Zangari, G.; Kirov, Y. Advanced alkaline water electrolysis. *Electrochim. Acta* **2012**, 82, 384–391.
- (5) Qi, J.; Zhang, W.; Cao, R. Solar-to-hydrogen energy conversion based on water splitting. *Adv. Energy Mater.* **2018**, 8, 1701620.
- (6) Cheng, F.; Chen, J. Metal-air batteries: from oxygen reduction electrochemistry to cathode catalysts. *Chem. Soc. Rev.* **2012**, 41, 2172–2192.
- (7) Suen, N. T.; Hung, S. F.; Quan, Q.; Zhang, N.; Xu, Y. J.; Chen, H. M. Electrocatalysis for the oxygen evolution reaction: recent development and future perspectives. *Chem. Soc. Rev.* **2017**, 46, 337–365.
- (8) Hong, W. T.; Risch, M.; Stoerzinger, K. A.; Grimaud, A.; Suntivich, J.; Shao-Horn, Y. Toward the rational design of non-precious transition metal oxides for oxygen electrocatalysis. *Energy Environ. Sci.* **2015**, 8, 1404–1427.
- (9) Matheu, R.; Garrido-Barros, P.; Gil-Sepulcre, M.; Ertem, M. Z.; Sala, X.; Gimbert-Suriñach, C.; Llobet, A. The development of molecular water oxidation catalysts. *Nat. Rev. Chem.* **2019**, 3, 331–341.
- (10) Najafpour, M. M.; Renger, G.; Holyńska, M.; Moghaddam, A. N.; Aro, E. M.; Carpentier, R.; Nishihara, H.; Eaton-Rye, J. J.; Shen, J. R.; Allakhverdiev, S. I. Manganese compounds as water-oxidizing catalysts: from the natural water-oxidizing complex to nanosized manganese oxide structures. *Chem. Rev.* **2016**, 116, 2886–936.
- (11) Park, S.; Lee, Y. H.; Choi, S.; Seo, H.; Lee, M. Y.; Balamurugan, M.; Nam, K. T. Manganese oxide-based heterogeneous electrocatalysts for water oxidation. *Energy Environ. Sci.* **2020**, 13, 2310–2340.
- (12) Shen, J. R. The structure of photosystem II and the mechanism of water oxidation in photosynthesis. *Annu. Rev. Plant Biol.* **2015**, 66, 23–48.
- (13) Britt, R. D.; Marchiori, D. A. Photosystem II, poised for O₂ formation. *Science* **2019**, 366, 305–306.
- (14) Askerka, M.; Brudvig, G. W.; Batista, V. S. The O₂-evolving complex of photosystem II: recent insights from quantum mechanics/molecular mechanics (QM/MM), extended X-ray absorption fine structure (EXAFS), and femtosecond X-ray crystallography data. *Acc. Chem. Res.* **2017**, 50, 41–48.
- (15) Vinyard, D. J.; Brudvig, G. W. Progress toward a molecular mechanism of water oxidation in photosystem II. *Annu. Rev. Phys. Chem.* **2017**, 68, 101–116.
- (16) Tanaka, A.; Fukushima, Y.; Kamiya, N. Two different structures of the oxygen-evolving complex in the same polypeptide frameworks of photosystem II. *J. Am. Chem. Soc.* **2017**, 139, 1718–1721.
- (17) Umena, Y.; Kawakami, K.; Shen, J. R.; Kamiya, N. Crystal structure of oxygen-evolving photosystem II at a resolution of 1.9 Å. *Nature* **2011**, 473, 55–60.
- (18) Yocum, C. The calcium and chloride requirements of the O₂ evolving complex. *Coord. Chem. Rev.* **2008**, 252, 296–305.
- (19) Yao, R.; Li, Y.; Chen, Y.; Xu, B.; Chen, C.; Zhang, C. Rare-earth elements can structurally and energetically replace the calcium in a synthetic Mn₄CaO₄-cluster mimicking the oxygen-evolving center in photosynthesis. *J. Am. Chem. Soc.* **2021**, 143, 17360–17365.
- (20) Pantazis, D. A. Missing pieces in the puzzle of biological water oxidation. *ACS Catal.* **2018**, 8, 9477–9507.
- (21) Suga, M.; Akita, F.; Sugahara, M.; Kubo, M.; Nakajima, Y.; Nakane, T.; Yamashita, K.; Umena, Y.; Nakabayashi, M.; Yamane, T.; Nakano, T.; Suzuki, M.; Masuda, T.; Inoue, S.; Kimura, T.; Nomura, T.; Yonekura, S.; Yu, L. J.; Sakamoto, T.; Motomura, T.; Chen, J. H.; Kato, Y.; Noguchi, T.; Tono, K.; Joti, Y.; Kameshima, T.; Hatsui, T.; Nango, E.; Tanaka, R.; Naitow, H.; Matsuura, Y.; Yamashita, A.; Yamamoto, M.; Nureki, O.; Yabashi, M.; Ishikawa, T.; Iwata, S.; Shen, J. R. Light-induced structural changes and the site of O=O bond formation in PSII caught by XFEL. *Nature* **2017**, 543, 131–135.
- (22) Kern, J.; Chatterjee, R.; Young, I. D.; Fuller, F. D.; Lassalle, L.; Ibrahim, M.; Gul, S.; Fransson, T.; Brewster, A. S.; Alonso-Mori, R.; Hussein, R.; Zhang, M.; Douthit, L.; de Lichtenberg, C.; Cheah, M. H.; Shevela, D.; Wersig, J.; Seuffert, I.; Sokaras, D.; Pastor, E.; Wening, C.; Kroll, T.; Sierra, R. G.; Aller, P.; Butryn, A.; Orville, A. M.; Liang, M.; Batyuk, A.; Koglin, J. E.; Carbajo, S.; Boutet, S.; Moriarty, N. W.; Holton, J. M.; Dobbek, H.; Adams, P. D.; Bergmann, U.; Sauter, N. K.; Zouni, A.; Messinger, J.; Yano, J.; Yachandra, V. K. Structures of the intermediates of Kok's photosynthetic water oxidation clock. *Nature* **2018**, 563, 421–425.
- (23) Suga, M.; Akita, F.; Yamashita, K.; Nakajima, Y.; Ueno, G.; Li, H.; Yamane, T.; Hirata, K.; Umena, Y.; Yonekura, S.; Yu, L. J.; Murakami, H.; Nomura, T.; Kimura, T.; Kubo, M.; Baba, S.; Kumazawa, T.; Tono, K.; Yabashi, M.; Isobe, H.; Yamaguchi, K.; Yamamoto, M.; Ago, H.; Shen, J. R. An oxyl/oxo mechanism for oxygen-oxygen coupling in PSII revealed by an X-ray free-electron laser. *Science* **2019**, 366, 334–338.
- (24) Pittkowski, R.; Krtil, P.; Rossmeisl, J. Rationality in the new oxygen evolution catalyst development. *Curr. Opin. Electrochem.* **2018**, 12, 218–224.
- (25) Rossmeisl, J.; Qu, Z. W.; Zhu, H.; Kroes, G. J.; Nørskov, J. K. Electrolysis of water on oxide surfaces. *J. Electroanal. Chem.* **2007**, 607, 83–89.
- (26) Man, I. C.; Su, H. Y.; Calle-Vallejo, F.; Hansen, H. A.; Martínez, J. I.; Inoglu, N. G.; Kitchin, J.; Jaramillo, T. F.; Nørskov, J. K.; Rossmeisl, J. Universality in oxygen evolution electrocatalysis on oxide surfaces. *ChemCatChem* **2011**, 3, 1159–1165.
- (27) Busch, M.; Ahlberg, E.; Panas, I. Water oxidation on MnO_x and IrO_x: why similar performance? *J. Phys. Chem. C* **2012**, 117, 288–292.
- (28) Zhao, Y.; Vargas-Barbosa, N. M.; Hernandez-Pagan, E. A.; Mallouk, T. E. Anodic deposition of colloidal iridium oxide thin films from hexahydroxyiridate(IV) solutions. *Small* **2011**, 7, 2087–2093.
- (29) Takashima, T.; Hashimoto, K.; Nakamura, R. Mechanisms of pH-dependent activity for water oxidation to molecular oxygen by MnO₂ electrocatalysts. *J. Am. Chem. Soc.* **2012**, 134, 1519–1527.
- (30) Gorlin, Y.; Jaramillo, T. F. A bifunctional nonprecious metal catalyst for oxygen reduction and water oxidation. *J. Am. Chem. Soc.* **2010**, 132, 13612–13614.
- (31) Zhou, F.; Izgorodin, A.; Hocking, R. K.; Spiccia, L.; MacFarlane, D. R. Electrodeposited MnO_x films from ionic liquid for electrocatalytic water

oxidation. *Adv. Energy Mater.* **2012**, 2, 1013–1021.

- (32) Mette, K.; Bergmann, A.; Tessonnier, J. P.; Hävecker, M.; Yao, L.; Ressler, T.; Schlögl, R.; Strasser, P.; Behrens, M. Nanostructured manganese oxide supported on carbon nanotubes for electrocatalytic water splitting. *ChemCatChem* **2012**, 4, 851–862.
- (33) Fekete, M.; Hocking, R. K.; Chang, S. L. Y.; Italiano, C.; Patti, A. F.; Arena, F.; Spiccia, L. Highly active screen-printed electrocatalysts for water oxidation based on β -manganese oxide. *Energy Environ. Sci.* **2013**, 6, 2222–2232.
- (34) Meng, Y.; Song, W.; Huang, H.; Ren, Z.; Chen, S. Y.; Suib, S. L. Structure-property relationship of bifunctional MnO_2 nanostructures: highly efficient, ultra-stable electrochemical water oxidation and oxygen reduction reaction catalysts identified in alkaline media. *J. Am. Chem. Soc.* **2014**, 136, 11452–11464.
- (35) Zhang, Y.; Chen, Y.; Liang, Z.; Qi, J.; Gao, X.; Zhang, W.; Cao, R. Controlled synthesis of hexagonal annular $\text{Mn}(\text{OH})\text{F}$ for water oxidation. *Chin. J. Catal.* **2019**, 40, 1860–1866.
- (36) Chen, Y.; Yang, S.; Liu, H.; Zhang, W.; Cao, R. An unusual network of α - MnO_2 nanowires with structure-induced hydrophilicity and conductivity for improved electrocatalysis. *Chin. J. Catal.* **2021**, 42, 1724–1731.
- (37) Smith, P. F.; Deibert, B. J.; Kaushik, S.; Gardner, G.; Hwang, S.; Wang, H.; Al-Sharab, J. F.; Garfunkel, E.; Fabris, L.; Li, J.; Dismukes, G. C. Coordination geometry and oxidation state requirements of corner-sharing MnO_6 octahedra for water oxidation catalysis: an investigation of manganite (γ - MnOOH). *ACS Catal.* **2016**, 6, 2089–2099.
- (38) Wan, S.; Li, Y.; Xu, L.; Zhang, W.; Cao, R. Autologous Mn oxides as electrocatalysts to identify the origin of the water oxidation activity. *Mater. Today Sustain.* **2022**, 17, 100106.
- (39) Huynh, M.; Shi, C.; Billinge, S. L.; Nocera, D. G. Nature of activated manganese oxide for oxygen evolution. *J. Am. Chem. Soc.* **2015**, 137, 14887–14904.
- (40) Kang, Q.; Vernisse, L.; Remsing, R. C.; Thenuwara, A. C.; Shumlas, S. L.; McKendry, I. G.; Klein, M. L.; Borguet, E.; Zdilla, M. J.; Strongin, D. R. Effect of interlayer spacing on the activity of layered manganese oxide bilayer catalysts for the oxygen evolution reaction. *J. Am. Chem. Soc.* **2017**, 139, 1863–1870.
- (41) Robinson, D. M.; Go, Y. B.; Mui, M.; Gardner, G.; Zhang, Z.; Mastrogianni, D.; Garfunkel, E.; Li, J.; Greenblatt, M.; Dismukes, G. C. Photochemical water oxidation by crystalline polymorphs of manganese oxides: structural requirements for catalysis. *J. Am. Chem. Soc.* **2013**, 135, 3494–3501.
- (42) Zhang, B.; Chen, H.; Daniel, Q.; Philippe, B.; Yu, F.; Valvo, M.; Li, Y.; Ambre, R. B.; Zhang, P.; Li, F.; Rensmo, H.; Sun, L. Defective and “c-disordered” hortensia-like layered MnO_x as an efficient electrocatalyst for water oxidation at neutral pH. *ACS Catal.* **2017**, 7, 6311–6322.
- (43) Park, J.; Kim, H.; Jin, K.; Lee, B. J.; Park, Y. S.; Kim, H.; Park, I.; Yang, K. D.; Jeong, H. Y.; Kim, J.; Hong, K. T.; Jang, H. W.; Kang, K.; Nam, K. T. A new water oxidation catalyst: lithium manganese pyrophosphate with tunable Mn valency. *J. Am. Chem. Soc.* **2014**, 136, 4201–4211.
- (44) Yoon, S.; Jin, K.; Lee, S.; Nam, K. T.; Kim, M.; Kwon, Y. K. Effects of paramagnetic fluctuations on the thermochemistry of $\text{MnO}(100)$ surfaces in the oxygen evolution reaction. *Phys. Chem. Chem. Phys.* **2021**, 23, 859–865.
- (45) Jiang, Y.; Yuan, L.; Wang, X.; Zhang, W.; Liu, J.; Wu, X.; Huang, K.; Li, Y.; Liu, Z.; Feng, S. Jahn-Teller disproportionation induced exfoliation

- of unit-cell scale ϵ - MnO_2 . *Angew. Chem. Int. Ed.* **2020**, 59, 22659–22666.
- (46) Thenuwara, A. C.; Cerkez, E. B.; Shumlas, S. L.; Attanayake, N. H.; McKendry, I. G.; Frazer, L.; Borguet, E.; Kang, Q.; Remsing, R. C.; Klein, M. L.; Zdilla, M. J.; Strongin, D. R. Nickel confined in the interlayer region of birnessite: an active electrocatalyst for water oxidation. *Angew. Chem. Int. Ed.* **2016**, 55, 10381–10385.
- (47) Cao, X.; Qiao, Y.; Jia, M.; He, P.; Zhou, H. Ion-exchange: a promising strategy to design Li-rich and Li-excess layered cathode materials for Li-ion batteries. *Adv. Energy Mater.* **2021**, 2003972.
- (48) Jin, K.; Park, J.; Lee, J.; Yang, K. D.; Pradhan, G. K.; Sim, U.; Jeong, D.; Jang, H. L.; Park, S.; Kim, D.; Sung, N. E.; Kim, S. H.; Han, S.; Nam, K. T. Hydrated manganese(II) phosphate ($\text{Mn}_3(\text{PO}_4)_2 \cdot 3\text{H}_2\text{O}$) as a water oxidation catalyst. *J. Am. Chem. Soc.* **2014**, 136, 7435–7443.
- (49) Kanan, M. W.; Nocera, D. G. In situ formation of an oxygen-evolving catalyst in neutral water containing phosphate and Co^{2+} . *Science* **2008**, 321, 1072–1075.
- (50) Liu, H.; Gao, X.; Yao, X.; Chen, M.; Zhou, G.; Qi, J.; Zhao, X.; Wang, W.; Zhang, W.; Cao, R. Manganese(II) phosphate nanosheet assembly with native out-of-plane Mn centres for electrocatalytic water oxidation. *Chem. Sci.* **2019**, 10, 191–197.
- (51) Yang, S.; Wan, S.; Shang, F.; Chen, D.; Zhang, W.; Cao, R. Autologous manganese phosphates with different Mn sites for electrocatalytic water oxidation. *Chem. Commun.* **2021**, 57, 6165–6168.
- (52) Takashima, T.; Hashimoto, K.; Nakamura, R. Inhibition of charge disproportionation of MnO_2 electrocatalysts for efficient water oxidation under neutral conditions. *J. Am. Chem. Soc.* **2012**, 134, 18153–18156.
- (53) Soldatova, A. V.; Romano, C. A.; Tao, L.; Stich, T. A.; Casey, W. H.; Britt, R. D.; Tebo, B. M.; Spiro, T. G. Mn(II) oxidation by the multicopper oxidase complex Mnx: a coordinated two-stage Mn(II)/(III) and Mn(III)/(IV) mechanism. *J. Am. Chem. Soc.* **2017**, 139, 11381–11391.
- (54) Gao, X.; Yang, S.; Zhang, W.; Cao, R. Biomimicking hydrogen-bonding network by ammoniated and hydrated manganese(II) phosphate for electrocatalytic water oxidation. *Acta Phys.-Chim. Sin.* **2021**, 37, 2007031.
- (55) Zaharieva, I.; Najafpour, M. M.; Wiechen, M.; Haumann, M.; Kurz, P.; Dau, H. Synthetic manganese-calcium oxides mimic the water-oxidizing complex of photosynthesis functionally and structurally. *Energy Environ. Sci.* **2011**, 4, 2400–2408.
- (56) Ramírez, A.; Bogdanoff, P.; Friedrich, D.; Fiechter, S. Synthesis of $\text{Ca}_2\text{Mn}_3\text{O}_8$ films and their electrochemical studies for the oxygen evolution reaction (OER) of water. *Nano Energy* **2012**, 1, 282–289.
- (57) Gonzalez-Flores, D.; Zaharieva, I.; Heidkamp, J.; Chernev, P.; Martinez-Moreno, E.; Pasquini, C.; Mohammadi, M. R.; Klingan, K.; Gernet, U.; Fischer, A.; Dau, H. Electrosynthesis of biomimetic manganese-calcium oxides for water oxidation catalysis-atomic structure and functionality. *ChemSusChem* **2016**, 9, 379–387.
- (58) Simchi, H.; Cooley, K. A.; Ohms, J.; Huang, L.; Kurz, P.; Mohny, S. E. Cosputtered calcium manganese oxide electrodes for water oxidation. *Inorg. Chem.* **2018**, 57, 785–792.
- (59) Park, S.; Jin, K.; Lim, H. K.; Kim, J.; Cho, K. H.; Choi, S.; Seo, H.; Lee, M. Y.; Lee, Y. H.; Yoon, S.; Kim, M.; Kim, H.; Kim, S. H.; Nam, K. T. Spectroscopic capture of a low-spin Mn(IV)-oxo species in $\text{Ni-Mn}_3\text{O}_4$ nanoparticles during water oxidation catalysis. *Nat. Commun.* **2020**, 11, 5230.
- (60) Huang, Z. F.; Song, J.; Dou, S.; Li, X.; Wang, J.; Wang, X. Strategies to break the scaling relation toward enhanced oxygen electrocatalysis.

Matter **2019**, 1, 1494–1518.

- (61) Geiger, S.; Kasian, O.; Ledendecker, M.; Pizzutilo, E.; Mingers, A. M.; Fu, W. T.; Diaz-Morales, O.; Li, Z.; Oellers, T.; Fruchter, L.; Ludwig, A.; Mayrhofer, K. J. J.; Koper, M. T. M.; Cherevko, S. The stability number as a metric for electrocatalyst stability benchmarking. *Nat. Catal.* **2018**, 1, 508–515.
- (62) Huang, Z. F.; Song, J.; Du, Y.; Xi, S.; Dou, S.; Nsanzimana, J. M. V.; Wang, C.; Xu, Z. J.; Wang, X. Chemical and structural origin of lattice oxygen oxidation in Co-Zn oxyhydroxide oxygen evolution electrocatalysts. *Nat. Energy* **2019**, 4, 329–338.
- (63) Koper, M. T. M. Theory of multiple proton-electron transfer reactions and its implications for electrocatalysis. *Chem. Sci.* **2013**, 4, 2710–2723.
- (64) Huang, Z. F.; Xi, S.; Song, J.; Dou, S.; Li, X.; Du, Y.; Diao, C.; Xu, Z. J.; Wang, X. Tuning of lattice oxygen reactivity and scaling relation to construct better oxygen evolution electrocatalyst. *Nat. Commun.* **2021**, 12, 3992.
- (65) Warren, J. J.; Tronic, T. A.; Mayer, J. M. Thermochemistry of proton-coupled electron transfer reagents and its implications. *Chem. Rev.* **2010**, 110, 6961–7001.
- (66) Ooka, H.; Takashima, T.; Yamaguchi, A.; Hayashi, T.; Nakamura, R. Element strategy of oxygen evolution electrocatalysis based on in situ spectroelectrochemistry. *Chem. Commun.* **2017**, 53, 7149–7161.
- (67) Balamurugan, M.; Saravanan, N.; Heonjin, H.; Lee, Y. H.; Nam, K. T. Involvement of high-valent manganese-oxo intermediates in oxidation reactions: realisation in nature, nano and molecular systems. *Nano Converg.* **2018**, 5, 18.
- (68) Kakizaki, H.; Ooka, H.; Hayashi, T.; Yamaguchi, A.; Bonnet-Mercier, N.; Hashimoto, K.; Nakamura, R. Evidence that crystal facet orientation dictates oxygen evolution intermediates on rutile manganese oxide. *Adv. Funct. Mater.* **2018**, 28, 1706319.
- (69) Wiechen, M.; Najafpour, M. M.; Allakhverdiev, S. I.; Spiccia, L. Water oxidation catalysis by manganese oxides: learning from evolution. *Energy Environ. Sci.* **2014**, 7, 2203–2212.
- (70) Zaharieva, I.; González-Flores, D.; Asfari, B.; Pasquini, C.; Mohammadi, M. R.; Klingan, K.; Zizak, I.; Loos, S.; Chernev, P.; Dau, H. Water oxidation catalysis-role of redox and structural dynamics in biological photosynthesis and inorganic manganese oxides. *Energy Environ. Sci.* **2016**, 9, 2433–2443.
- (71) Huynh, M.; Bediako, D. K.; Nocera, D. G. A functionally stable manganese oxide oxygen evolution catalyst in acid. *J. Am. Chem. Soc.* **2014**, 136, 6002–6010.
- (72) Zahran, Z. N.; Mohamed, E. A.; Naruta, Y. Kinetics and mechanism of heterogeneous water oxidation by α -Mn₂O₃ sintered on an FTO electrode. *ACS Catal.* **2016**, 6, 4470–4476.
- (73) Wang, N.; Zheng, H.; Zhang, W.; Cao, R. Mononuclear first-row transition-metal complexes as molecular catalysts for water oxidation. *Chin. J. Catal.* **2018**, 39, 228–244.

(74) Jin, X.; Li, X.; Lei, H.; Guo, K.; Lv, B.; Guo, H.; Chen, D.; Zhang, W.; Cao, R. Comparing electrocatalytic hydrogen and oxygen evolution activities of first-row transition metal complexes with similar coordination environments. *J. Energy Chem.* **2021**, 63, 659–666.

(75) Cao, R.; Lai, W.; Du, P. Catalytic water oxidation at single metal sites. *Energy Environ. Sci.* **2012**, 5, 8134–8157.

(76) Li, X.; Lei, H.; Xie, L.; Wang, N.; Zhang, W.; Cao, R. Metalloporphyrins as catalytic models for studying hydrogen and oxygen evolution and oxygen reduction reactions. *Acc. Chem. Res.* **2022**, DOI:10.1021/acs.accounts.1c00753.

(77) Zhang, X. P.; Wang, H. Y.; Zheng, H.; Zhang, W.; Cao, R. O–O bond formation mechanisms during the oxygen evolution reaction over synthetic molecular catalysts. *Chin. J. Catal.* **2021**, 42, 1253–1268.

(78) Zhang, X. P.; Chandra, A.; Lee, Y. M.; Cao, R.; Ray, K.; Nam, W. Transition metal-mediated O–O bond formation and activation in chemistry and biology. *Chem. Soc. Rev.* **2021**, 50, 4804–4811.

(79) Li, X.; Zhang, X. P.; Guo, M.; Lv, B.; Guo, K.; Jin, X.; Zhang, W.; Lee, Y. M.; Fukuzumi, S.; Nam, W.; Cao, R. Identifying intermediates in electrocatalytic water oxidation with a manganese corrole complex. *J. Am. Chem. Soc.* **2021**, 143, 14613–14621.

(80) Lai, W.; Cao, R.; Dong, G.; Shaik, S.; Yao, J.; Chen, H. Why is cobalt the best transition metal in transition-metal handman corroles for O–O bond formation during water oxidation? *J. Phys. Chem. Lett.* **2012**, 3, 2315–2319.

(81) Lei, H.; Liu, C.; Wang, Z.; Zhang, Z.; Zhang, M.; Chang, X.; Zhang, W.; Cao, R. Noncovalent Immobilization of a pyrene-modified cobalt corrole on carbon supports for enhanced electrocatalytic oxygen reduction and oxygen evolution in aqueous solutions. *ACS Catal.* **2016**, 6, 6429–6437.

(82) Seo, H.; Jin, K.; Park, S.; Cho, K. H.; Ha, H.; Lee, K. G.; Lee, Y. H.; Nguyen, D. T.; Randriamahazaka, H.; Lee, J. S.; Nam, K. T. Mechanistic investigation with kinetic parameters on water oxidation catalyzed by manganese oxide nanoparticle film. *ACS Sustain. Chem. Eng.* **2019**, 7, 10595–10604.

(83) Lee, J.; Choe, I. R.; Kim, Y. O.; Namgung, S. D.; Jin, K.; Ahn, H. Y.; Sung, T.; Kwon, J. Y.; Lee, Y. S.; Nam, K. T. Proton conduction in a tyrosine-rich peptide/manganese oxide hybrid nanofilm. *Adv. Funct. Mater.* **2017**, 27, 1702185.

(84) Lee, K. G.; Balamurugan, M.; Park, S.; Ha, H.; Jin, K.; Seo, H.; Nam, K. T. Importance of entropic contribution to electrochemical water oxidation catalysis. *ACS Energy Lett.* **2019**, 4, 1918–1929.

Received: February 17, 2022

Accepted: March 12, 2022

Published: April 8, 2022